JOURNAL OF GEOPHYSICAL RESEARCH, VOL. 101, NO. A12, PAGES 26,681–26,696, DECEMBER 1, 1996

Assimilative mapping of ionospheric electrodynamics in the thermosphere-ionosphere general circulation model comparisons with global ionospheric and thermospheric observations during the GEM/ SUNDIAL period of March 28-29, 1992

B. A. Emery, [1] G. Lu, [1] E. P. Szuszczewicz, [2] A. D. Richmond, [1] R. G. Roble, [1] P. G. Richards, [3] K. L. Miller, [4] R. Niciejewski, [5] D. S. Evans, [6] F. J. Rich, [7] W. F. Denig, [7] D. L. Chenette, [8] P. Wilkinson, [9] S. Pulinets, [10] K. F. O'Loughlin, [11] R. Hanbaba, [12] M. Abdu, [13] P. Jiao, [14] K. Igarashi, [15] and B. M. Reddy [16]

Abstract. Satellite and ground-based observations from March 28 to 29, 1992, were combined in the assimilative mapping of ionospheric electrodynamics (AMIE) procedure to derive realistic global distributions of the auroral precipitation and ionospheric convection which were used as inputs to the National Center for Atmospheric Research (NCAR) thermosphere-ionosphere general circulation model (TIGCM). Comparisons of neutral model winds were made with Fabry-Perot measurements and meridional winds derived from ionosondes. The peak equatorward winds occurred 1–2 hours later in the model. Gravity waves launched from high-latitude Joule heating sources reached the equator in about 2 hours and agreed with observed variations in the height of the maximum electron density ($hmF2$) and in the meridional winds. Joule heating events produced minima in the O/N_2 ratio that moved equatorward and usually westward in longitudinal strips which lasted about a day. Changes in the O/N_2 ratio and in the peak electron density ($NmF2$) were strongly correlated so the observed daytime $NmF2$ values for stations near 50° magnetic latitude were generally reproduced by AMIE-TIGCM on the second day of the simulation. The AMIE-TIGCM underestimated the electron density after midnight by up to a factor of 2 in midlatitudes, while the modeled $F2$ layer was about 35 km lower than the observations at midnight. Shifting the model winds 2 hours earlier at night could double the $NmF2$ at 0400 LT and increase $hmF2$ by 20 km. $NmF2$ could also be increased at night by realistically increasing the TIGCM nighttime downward fluxes of O^+ at the upper boundary.

[1]High Altitude Observatory, National Center for Atmospheric Research, Boulder, Colorado.

[2]Laboratory for Atmospheric and Space Science, Science Applications International Corporation, McLean, Virginia.

[3]Computer Science Department, University of Alabama, Huntsville.

[4]Center for Atmospheric and Space Sciences, Utah State University, Logan.

[5]Space Physics Research Laboratory, University of Michigan, Ann Arbor.

[6]Space Environment Center, National Oceanic and Atmospheric Administration, Boulder, Colorado.

[7]Geophysics Directorate, Phillips Laboratory, Hanscom Air Force Base, Massachusetts.

[8]Lockheed Palo Alto Research Laboratory, Palo Alto, California.

[9]IPS Radio and Space Services, West Chatswood, Australia.

[10]Institute of Terrestrial Magnetism, Ionosphere and Radiowave Propagation, IZMIRAN, Moscow Region, Troitsk.

[11]National Geophysical Data Center, National Oceanic and Atmospheric Administration, Boulder, Colorado.

[12]Centre National d'Etudes des Télécommunications, Lannion, France.

[13]Divisao de Aeronomia, Instituto Nacional de Pesquisas Espaciais, Sao Jose dos Campos, Brazil.

[14]China Research Institute of Radiowave Propagation, Xinxiang, Henan.

[15]Upper Atmosphere Section, Communications Research Laboratory, Ministry of Posts and Telecommunications, Tokyo, Japan.

[16]Radio Science Division, National Physical Laboratory, New Delhi, India.

Copyright 1996 by the American Geophysical Union.

Paper number 96JA01285.
0148-0227/96/96JA-01285$09.00

Introduction

Many observations were collected during the solar maximum period of March 28–29, 1992, as one of the Geospace Environment Modeling (GEM) observational campaigns. A major goal of the GEM program is to understand the solar/magnetosphere/ionosphere coupling processes well enough so that models can be built for use in space weather applications. This GEM campaign was a part of the 12-day SUNDIAL period of March 24 to April 4. A goal of the SUNDIAL program is to develop an improved quantitative understanding of the global ionosphere/thermosphere system and to test and validate productive capabilities using empirical and first principles models and a worldwide database of primarily ionosonde measurements. High-latitude global observations were used as inputs to the assimilative mapping of ionospheric electrodynamics (AMIE) model to define the ion convection [e.g., *Richmond et al.*, 1988; *Knipp et al.*, 1993]. The AMIE technique also includes fitting the height-integrated Hall and Pedersen conductance in order to utilize ground magnetometer data [*Richmond and Kamide*, 1988]. This paper will discuss the expansion of the AMIE fitting procedure to include separate fits for the auroral energy flux and mean energy, which have only been lightly touched upon in the literature [*Knipp et al.*, 1993; *Lu et al.*, 1995]. These auroral parameters are essential inputs to the thermosphere-ionosphere general circulation model (TIGCM). Global ionospheric and thermospheric observations in this period will then be compared to the AMIE-TIGCM calculations.

In a companion paper, *Lu et al.* [this issue] describe the high-latitude electrodynamics as determined by the AMIE procedure using data every 5 min for March 28–29, 1992. A previous paper [*Lu et al.*, 1995] used a reduced data set in AMIE as input to the TIGCM. The present paper uses the expanded data set but concentrates on universal times with the maximum data coverage and averages all data for those periods over ±17.5 min (or 35 min). This results in smoother convection patterns and less temporal variability, much of which is due to intermittent data coverage by satellites. Variability in the Joule heating produces gravity waves in the high-latitude regions that propagate equatorward [e.g., *Roble et al.*, 1987; *Fesen et al.*, 1989; *Crowley et al.*, 1989a]. It is thus desirable to eliminate as many spurious gravity wave sources as possible in the TIGCM, especially when gravity waves are part of the study.

The resulting AMIE patterns were in turn averaged in order to provide "climatological" southern and northern hemisphere average patterns that were used to initialize the TIGCM run. The companion paper by *Szuszczewicz et al.* [this issue] used a 24-hour TIGCM run of this climatological average to compare against other models and ionosonde data averaged over the 12-day campaign period. The present study concentrates on the daily variations for March 28–29 only and compares the daily variability to the averages.

March 28–29, 1992, was in the declining phase of the solar cycle, with 10.7-cm solar fluxes of 185 and 192, respectively. Magnetic activity began on March 21 with a sudden storm commencement followed by a sequence of smaller storms. The only quiet day was April 2, with March 28 being the next quietest period with a daily *Ap* of 10. March 29 was the third most disturbed day of the period with a daily *Ap* of 18. The *Kp* varied between 2 and 4- for March 28–29, and between 1- and 6 for the whole period. Therefore the 12-day average ionosonde data could be considered to be a disturbed average.

In general, the peak electron density $NmF2$ is reduced in midlatitudes following a single isolated storm due to an increase in the N_2/O ratio (or a decrease in the O/N_2 ratio), while it is usually increased at low latitudes due to equatorward winds, although electric field effects can have a negative or positive effect [e.g., *Prölss*, 1995, and references therein]. Individual magnetic storms can be either "positive" or "negative" according to whether $NmF2$ is increased or decreased from mean quiet day values. The negative storm effects caused by decreases in the O/N_2 ratio can lag the storm by nearly a day and are sensitive to the storm intensity, the season, geographic and geomagnetic coordinates, and the local time at which the main phase of the magnetic storm begins. A study of a 10-day period by *Codrescu et al.* [1992] showed that the negative effects on $NmF2$ at 45°N magnetic latitude can last at least 6 days after an initial storm. There are positive and negative variations in the disturbed period embedded within the context of the general negative response. Since our period is shorter and does not cover the beginning of the magnetic activity, we will only be looking at these relative positive and negative variations within the larger context of a disturbed period.

We will compare neutral winds, first with Fabry-Perot measurements, and second with winds derived from ionosonde measurements of $hmF2$, noting evidence of gravity waves. We will look at $NmF2$ variations from the polar cap to the equator and concentrate on the higher midlatitude region where O/N_2 differences can cause large changes in the daytime peak electron density. The question of the maintenance of the nighttime density will be examined with another AMIE-TIGCM run with realistic increased downward fluxes of O^+ at the upper boundary at night.

Specifying the Auroral Inputs

The auroral inputs of the mean Maxwellian energy and the energy flux of precipitating electrons are necessary components to the TIGCM. They are normally parameterized in a circular precipitation region as described by *Roble and Ridley* [1987], where the characteristics of this simple oval are defined by the hemispheric power index [*Fuller-Rowell and Evans*, 1987]. However, it is better to include a more realistic pattern of the auroral inputs from the AMIE results for campaign studies. AMIE uses magnetic apex coordinates [*VanZandt et al.*, 1972], which are also used in this paper to refer to individual locations. The TIGCM uses a simple dipole field.

The first attempt to use AMIE inputs in the thermosphere general circulation model (TGCM) [*Dickinson et*

al., 1984] was described by *Crowley et al.* [1989a], where patterns of the electric potential were put in, but the aurora was still based on the simple parameterization of *Roble and Ridley* [1987] modified by the available electron precipitation data. The present AMIE procedure now solves the auroral energy flux and mean electron energy explicitly. The AMIE data-fitting algorithms we use for energy flux and mean energy are entirely analogous to those described by *Richmond and Kamide* [1988] for fitting conductance observations. That is, for both the flux and the mean energy we determine a modifying function needed to multiply an empirical model in order to make the empirical model agree more closely with actual point observations. The modifying function is obtained by performing an optimal linear estimation fit to logarithms of ratios of observations to empirical model values, using constraints to obtain a smooth fit consistent with general properties of observed electron precipitation. The empirical energy flux model is that of *Fuller-Rowell and Evans* [1987], parameterized by the 10-level hemispheric power index. The empirical mean energy model is obtained from the Hall-to-Pedersen ratio of the *Fuller-Rowell and Evans* [1987] auroral conductance models by finding a Maxwellian distribution that produces the same ratio (T. J. Fuller-Rowell, private communication, 1992). The initial estimates of the hemispheric power index are taken in this study from estimates of the hemispheric power in GW provided by four Defense Meteorological Satellite Program (DMSP) satellites: F08, F09, F10, and F11.

The conductance sources for this period [see *Lu et al.*, this issue] came from electron precipitation measurements from four DMSP satellites [*Rich et al.*, 1987] and NOAA 12 [*Fuller-Rowell and Evans*, 1987], plus X ray measurements from the Upper Atmospheric Research Satellite (UARS) [*Chenette et al.*, 1993]. Further conductance estimates revised from *Ahn et al.* [1983] (B.-H. Ahn, private communication, 1991) use ground magnetometer observations in auroral regions which contain both auroral and solar ultraviolet (UV) influences. If the model UV component is less than the model auroral component, the solar UV component is subtracted from the observation, and the inverse of the formulas in the work of *Robinson et al.* [1987] are used to convert the remaining Hall and Pedersen auroral conductance to auroral electron energy flux and mean energy.

The satellite observations are more direct observations of the auroral energy flux and electron mean energy. The Maxwellian energy and energy flux of precipitating electrons are extracted from the X ray spectrum for energies above about 3 keV [*Chenette et al.*, 1993]. For NOAA 12, auroral energy fluxes are integrated over the instrument span of 300 eV to 20 keV [*Fuller-Rowell and Evans*, 1987], while for DMSP, these are integrated over 460 eV to 30 keV [*Rich et al.*, 1987]. The mean electron energy is the simple ratio of the energy flux over the number flux in this energy range for DMSP satellites, and this distribution function is assumed to be Maxwellian. The characteristic energy from the NOAA satellite is related to a particular Hall-to-Pedersen ratio, which in turn is assigned to a Maxwellian distribution that produces the same peak ionization. Error bars are usually standard deviations plus increasing errors for data taken at times progressively further away from the time of the calculation.

Conjugacy is usually assumed for fitting the auroral parameters or conductance since this is a fairly good assumption for large-scale features of the aurora [e.g. *Mizera and Evans*, 1986]. However, the error bar in the conjugate hemisphere is increased an extra 50%. Figure 1 illustrates the procedure for the northern hemisphere for 0755 UT on March 28, 1992. The hemispheric

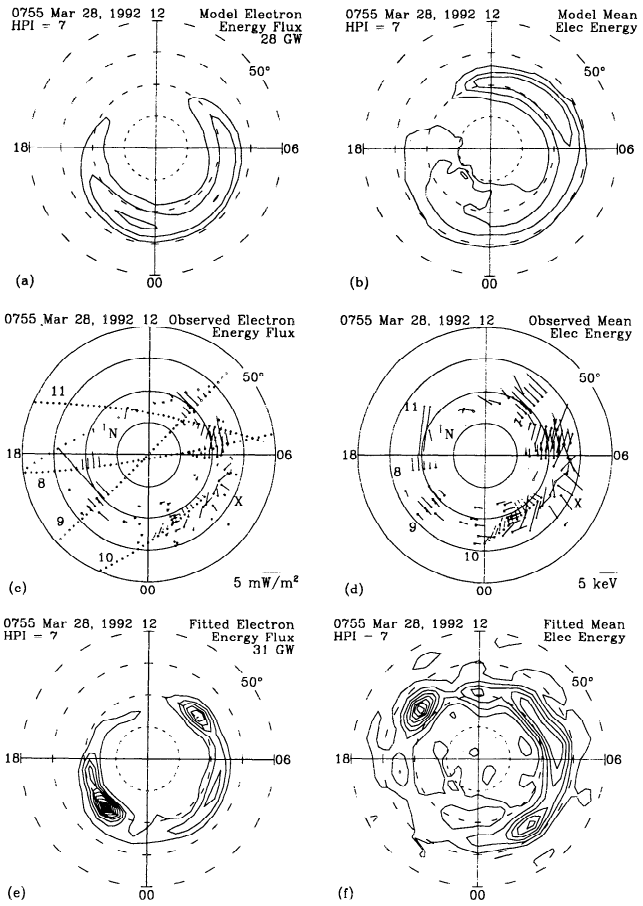

Figure 1. (a) Electron energy flux in contour intervals of 1 mW/m^2 from the *Fuller-Rowell and Evans* [1987] pattern for a hemispheric power index of 7 as a function of magnetic latitude and local time. (b) Mean Maxwellian energy of the auroral electrons based on the Hall-to-Pedersen ratio at the hemispheric power level of 7 in contour intervals of 1 keV starting at 3 keV. (c) Observations of the energy flux in mW/m^2 between 0738 and 0812 UT on March 28, 1992, from the DMSP F08, F09, F10, and F11 satellites (marked with 8, 9, 10, 11), the NOAA 12 satellite (N), the UARS AXIS X ray imager (X), and ground magnetometers (x). The satellite estimates are marked with open circles if they are before 0755 UT, and marked with a plus if they are after 0755 UT. (d) Same as Figure 1c except for the mean electron energy. (e) Fitted electron energy flux in mW/m^2 from the AMIE procedure for 0755 UT on March 28, 1992. (f) Same as Figure 1c except for the mean electron energy.

power determined from the DMSP F09 and F08 passes centered at 0747 and 0800 UT are 34.6 and 23.9 GW, respectively, leading to an average of 28 GW at 0755, which corresponds to a hemispheric power index of 7. Figure 1a shows the statistical model distribution of energy flux obtained from *Fuller-Rowell and Evans* [1987] for this level of auroral precipitation. The hemispheric integration of this flux is 28 GW, which is coincidentally the same hemispheric power as the original estimate. Figure 1b is the mean Maxwellian energy derived from the conductance ratio at level 7. Figures 1c and 1d show the observations, where the mean energies are only plotted if the associated energy flux is greater than 0.3 mW/m. The orbits for NOAA and DMSP are marked, while the UARS track samples between 0100 and 0800 LT and between 60° and 70°N. The dashed lines on the F10 orbit indicate that it was in the southern hemisphere at the time. Figures 1e and 1f show the AMIE-fitted distributions, where the average hemispheric power estimated from the energy flux in Figure 1e is 31 GW. The estimated patterns derived in Figures 1e and 1f clearly reflect the influence of the data and are different from the initial statistical patterns of Figures 1a and 1b.

Putting AMIE Outputs Into the TIGCM

The original NCAR TGCM described by *Dickinson et al.* [1981, 1984] calculates the thermospheric neutral dynamics, temperature, and composition. This model has been used extensively in data comparisons [e.g., *Hernandez and Roble*, 1976; *Forbes et al.*, 1987; *Crowley et al.*, 1989b; *Fesen et al.*, 1986]. The TGCM was also used by *Fesen et al.* [1989] along with an equatorial model of the ionosphere to show that most of the storm time variations in the equatorial anomaly could be explained by the neutral winds that exhibited waves that propagated from high latitudes to the equator. The TIGCM is an extension of the TGCM that self-consistently solves for the ionospheric composition and temperatures [*Roble et al.*, 1988]. The updated metastable chemistry is described by *Roble* [1995]. Comparisons of the TIGCM have been used to study descending ionization layers [*Wilkinson et al.*, 1992] and O/N_2 ratios related to magnetic storms [*Burns et al.*, 1995a, b]. *Codrescu et al.* [1992] used the TIGCM along with northern hemisphere ionosondes between 15° and 50°N magnetic latitude near 130°E geographic longitude to look at relative differences during a solar maximum storm period in March 1979. The relative changes in the height and peak electron density following the initial storm on March 22 were in fairly good agreement at 45°N magnetic latitude, but the agreement degraded further equatorward. However, in conjuction with the companion paper of *Szuszczewicz et al.* [this issue], the present study is the first attempt to make direct, rather than relative, comparisons with ionosonde data using the TIGCM.

The required inputs for the TIGCM are specified semidiurnal tides at the bottom boundary, O^+ fluxes at the top boundary (near 550 km for this period), solar EUV and UV fluxes, electric fields, and the auroral electron precipitation flux and Maxwellian energy. The midlatitude and low-latitude electric fields are specified by the empirical model of *Richmond et al.* [1980], while the high-latitude electric fields and the auroral parameters are specified in this study with the AMIE outputs. The time-averaged AMIE patterns over March 28–29 were used in the *Szuszczewicz et al.* [this issue] study. The present study uses the output of that simulation at 2400 UT as the initial conditions for our simulation with time-varying AMIE inputs. Because the averages are similar to the conditions at 0000 UT on March 28, the transition from the initial state to the campaign period is relatively smooth.

The 2-day period of March 28–29, 1992, was simulated in the TIGCM using 66 northern hemisphere and

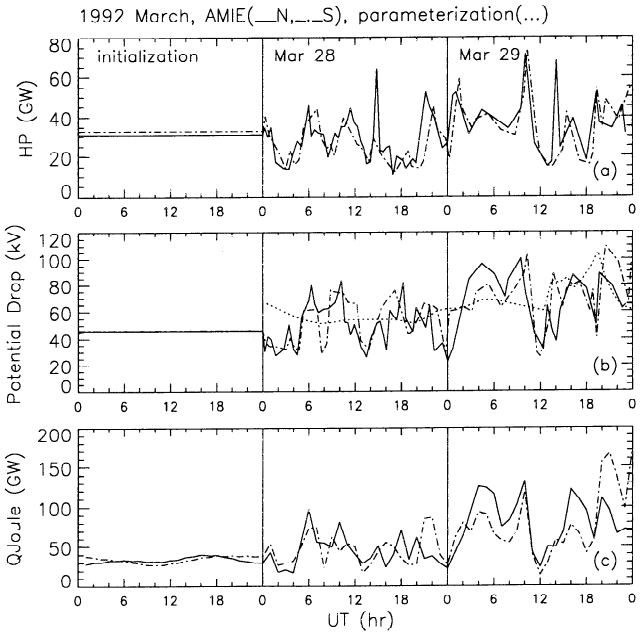

Figure 2. (a) Hemispheric power in GW derived from the AMIE procedure for 66 northern hemisphere (solid) patterns and 53 southern hemisphere (dotted-dashed) patterns for March 28–29, 1992. The first 24 hours is the average of these patterns used as the 24-hour initialization run in the TIGCM. (b) Like Figure 2a except this is the cross-tail potential drop in kilovolts derived from the AMIE procedure. The dotted line is the cross-tail potential drop determined from the solar wind speed and the interplanetary magnetic field (IMF) from *Reiff and Luhmann* [1986] between 1300 and 2000 UT on March 29, 1992. At other universal times, it is estimated from *Kp* (P. H. Reiff, private communication, 1985) for March 28–29, 1992. (c) Hemispheric Joule heating rate estimates in GW calculated from the TIGCM at every hour for the northern (solid) and southern (dashed-dotted) hemispheres when using the AMIE patterns for March 28–29, 1992, and the time-averaged AMIE patterns for the first 24 hours. The effects of the neutral winds are included.

53 southern hemisphere AMIE patterns of auroral energy flux, mean electron energy, and electric potential (i.e., convection). Figure 2 shows the hemispheric power estimated from the auroral energy flux fits as described in the previous section along with the AMIE polar cap potential drops. These curves roughly track the outer envelop of values shown in Figures 7b and 7c of the companion paper of *Lu et al.* [this issue]. The time-averaged AMIE used as the initialization period are shown as straight lines and do not represent the real conditions before March 28. The average pattern of precipitating electron flux was similar to the statistical model plotted in Figure 1a, except for less flux near midnight as shown in Figure 1e. The time-averaged mean energy was also similar to the statistical model plotted in Figure 1b, apart from lower energies of about 3.5 keV in the premidnight sector similar to Figure 1f. The average hemispheric power for the initialization period is about 31–33 GW, which is about the same as the average over March 28–29.

The time-averaged convection pattern in the southern hemisphere exhibited a large, round negative electric potential cell in the evening with a small crescent-shaped dayside positive potential cell consistent with a negative interplanetary magnetic field (IMF) B_y such as was measured during the period of available IMF on March 29 [*Lu et al.*, this issue]. In the northern hemisphere, the two cells were more symmetric. The polar cap potential drop of the averaged patterns was 46 kV in both hemispheres. The average potential drop of the 43 patterns on March 28 was 50 kV, while the average for the 23 patterns on March 29 was 65 kV. This illustrates that averaging different convection patterns in magnetic local time and magnetic latitude has the effect of smoothing them and reducing the extrema, resulting in a single pattern with a lower polar cap potential drop (46 kV). As a comparison, the dotted line in Figure 2b shows the polar cap potential drop determined from the available hourly IMF and solar wind velocity between 1300 and 2000 UT on March 29 according to the formula of *Reiff and Luhmann* [1986], and estimated from Kp [*Reiff et al.*, 1981; P. H. Reiff, private communication, 1985] at other times. In the absence of AMIE inputs, this is the potential drop that would be used in the TIGCM along with the IMF B_y to specify convection parameters from *Heelis et al.* [1982]. However, as can be seen in Figure 2b, the temporal variations of the potential drop so estimated are quite different from the AMIE results even during the period of available IMF. This has profound consequences for the timing and location of Joule heating events since the Joule heating hemispheric averages calculated in the TIGCM and plotted in Figure 2c generally follow the polar cap potential drops in Figure 2b.

The cross-tail potential drop for the time-averaged convection in Figure 2b for the initialization period is nearly identical for both hemispheres, but in Figure 2c, it is apparent that the TIGCM Joule heating rate is up to 10 GW larger in the southern hemisphere between 1900 and 0500 UT and up to 5 GW larger in the northern hemisphere between 0600 and 1800 UT. A TIGCM run made with the parameterized IMF and Kp potential drop shown in Figure 2b for March 28–29 showed similar results, with up to 15–20 GW larger Joule heating rates in one or the other hemisphere, with the largest differences at times of the largest potential drops on March 29. The north magnetic pole is tilted toward the Sun around 1600 UT, thus increasing the area of the convection exposed to sunlight. *Lu et al.* [this issue] found a similar universal time effect in Joule heating using the time-varying AMIE patterns assuming the neutral winds to be zero.

Data/Model Comparisons With Fabry-Perot Observations

There have been many previous comparisons of Fabry-Perot interferometer (FPI) measurements of nighttime neutral winds and temperatures using the 630-nm emission of atomic oxygen with the TGCM and TIGCM [e.g., *Hernandez and Roble*, 1976, 1995]. The nominal height of the emission layer is 250 km, but it can be lower in the presence of aurora. Figure 3 shows the observations and comparisons with both model runs for Watson Lake (60.1°N, 231.4°E) which is located at a magnetic latitude of 64°N. Inspection of the AMIE plots of the auroral electron energy flux show that Watson Lake is generally in or close to the equatorward part of the fitted auroral oval all night.

The brightness measurements plotted in Figure 3a were in relative units and so have been adjusted to be approximately the same as the AMIE-TIGCM predawn levels. These observations show enhancements at 1000 UT on March 28, and between 0400–0500 UT and 0800–1000 UT on March 29. The AMIE-TIGCM run shows modest increases in brightness especially between 0800 and 1000 UT on March 29. The TIGCM grid is 5° in both geographic latitude and geographic longitude and thus cannot be expected to reproduce small-scale local auroral features such as may be involved here, although the increased calculated brightness indicates that Watson Lake was fairly close to the auroral oval in the TIGCM simulation.

The increased brightness observations in Figure 3a correlate with decreases in the neutral temperature shown in Figure 3b and are a reflection of nearby auroral emissions which come from lower altitudes than do the airglow emissions. The TIGCM temperatures are averages based on the calculated emission as a function of height [*Hernandez and Roble*, 1995], but they are close to the temperatures at 250 km in the absence of auroral precipitation. The average observed temperature in the enhanced brightness regions is about 800 K, compared to values about 1100 K before and afterward. A nighttime temperature of 800 K above Watson Lake in the AMIE-TIGCM corresponds roughly to a height of 160 km. The peak altitude of 630-nm emission is 170 km for a Maxwellian spectrum with mean electron energy of 4 keV [*Rees and Roble*, 1986], compatible with the mean energy inferred from the AMIE results.

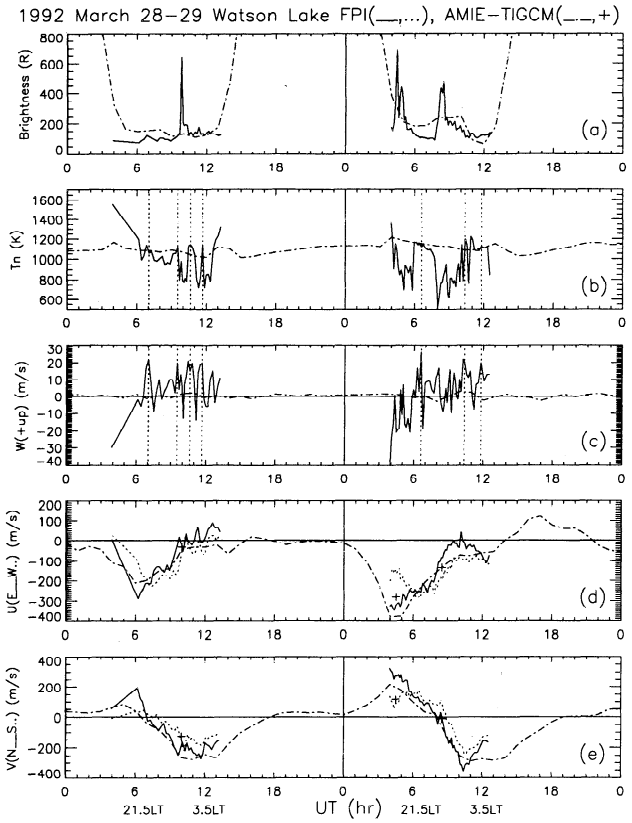

Figure 3. Fabry-Perot 630-nm observations on March 28–29, 1992, above Watson Lake, Canada. The AMIE-TIGCM results are plotted as a dotted-dashed line. (a) Brightness in rayleighs from observations overhead compared to model results. The observations in arbitrary units of relative brightness were multiplied by 30. (b) Neutral temperature in kelvin from overhead compared to model results. (c) Vertical wind looking directly above the station positive upward in meters per second compared to AMIE-TIGCM results. The dotted lines here and in Figure 3b mark the times where the upward velocity is larger than 20 m/s. (d) Zonal neutral wind in meters per second positive toward geographic east looking east (solid) and west (dotted) compared to model values. The pluses are model values at 160 km. (e) Meridional neutral wind in meters per second positive toward geographic north looking north (solid) and south (dotted) compared to model results.

Figure 3c shows the vertical wind observations against the AMIE-TIGCM calculations. The observations are much larger than the model because the global grid scale of the TIGCM does not allow large divergences and convergences in the horizontal winds to develop that couple into the vertical wind. However, large vertical winds are a common feature of FPI observations [e.g., *Sipler et al.*, 1995; *Price et al.*, 1995; *Smith and Hernandez*, 1995]. The vertical velocity appears to oscillate with a periodicity of about an hour, especially on March 28, and may be an indication of gravity waves. The peaks in the vertical velocity sometimes correspond to peaks in the temperature as shown by the dotted vertical lines in Figures 3b and 3c.

The overhead neutral zonal and meridional winds above Watson Lake obtained from the AMIE-TIGCM run are plotted in Figures 3d and 3e as well as observations at Watson Lake from the look directions to the east and west, and to the north and south, at an elevation angle of 45°. For an emission layer at 250 km, this corresponds to a horizontal distance of 250 km. The goodness of the comparison between the observations and AMIE-TIGCM results can often be improved by adjusting the emission height at the universal times of the strongest brightness observations in Figure 3a. The revised AMIE-TIGCM velocities are shown as pluses in Figures 3d and 3e. The observed equatorward winds in Figure 3e peak between 1000 and 1200 UT (0126 and 0326 LT), which is somewhat earlier than the peak AMIE-TIGCM equatorward winds.

Data/Model Comparisons With Ionosonde Observations

The excellent review of ionospheric F region storms by *Prölss* [1995] describes a few important mechanisms that explain most storm effects on the electron density. Most midlatitude effects are negative with density losses due to decreases in the O/N_2 ratio on both constant altitude and pressure surfaces. *Burns et al.* [1995a, b] studied this extensively using the TIGCM and DE 2 satellite data. The decrease on constant pressure surfaces is usually due to both increases in N_2 which increases the loss of O^+ and decreases in O which decreases the daytime production of O^+. According to *Prölss* [1995], positive storm effects could be related to composition changes, but are attributed mainly to upward drifts due to equatorward winds usually associated with gravity waves that show as increases in $hmF2$. The positive storm effects due to increases in $hmF2$ are daytime only due to the presence of solar ionization. Also important in both positive and negative storm effects are electric fields which are either external (of magnetospheric origin) or created by dynamo winds [e.g., *Blanc and Richmond*, 1980].

There have been several studies that have compared first principles models with ionosonde observations. *Wilkinson et al.* [1988] used the Utah State University model with model auroral inputs and neutral composition and found, as did *Szuszczewicz et al.* [this issue], that the agreement between model and observations is usually worse at night, with the model electron densities much lower than the observations. Another study by *Sica et al.* [1990] showed that agreement between the Utah State model and ionosonde $NmF2$ measurements at night could be achieved either with equatorward winds or with a reasonable downward flux of O^+ at 1000 km, or both.

Comparisons were made with data from the 53 ionosonde stations listed in Table 1 of *Szuszczewicz et al.* [this issue] plus the American stations of Boulder and Wallops Island. All stations provided hourly $foF2$ data, which is the critical frequency of the ordinary ionosonde trace with typical error bars of 0.1 MHz [*Wilkinson*,

1978]. This is related to the peak electron density ($NmF2$) by the following relationship:

$$foF2(Hz) = 0.9 \times \sqrt{NmF2(m^{-3})} \qquad (1)$$

Thirty-six stations also provided values of the transmission factor $M(3000)F2$, making it possible to determine the height ($hmF2$) of the peak electron density using the method of *Dudeney* [1983], where typical error bars are about ±10 km with extreme error bars of ±30 km during times of spread F [*Wilkinson et al.*, this issue]. Neutral meridional winds positive towards magnetic north were then derived from $hmF2$ using the servo-analysis technique of *Miller et al.* [1986, 1993]. The servo-analysis of $hmF2$ assumes mass spectrometer incoherent scatter (MSIS) model neutral temperatures and composition [e.g., *Hedin*, 1991] to produce an effective wind composed of the neutral wind plus electric field effects. Hence the meridional wind estimates are not used above 60° magnetic or below 20° since electric fields are expected to be important in high and low latitudes. A ±20 km error in $hmF2$ will result in ±25 m/s errors in the ionosonde winds at night, and ±50 m/s errors during the afternoon.

High and Low Latitudes

Figure 4 shows the electron density peak and the $hmF2$ values for several stations at high and low latitudes where electric fields are expected to be important. Vertical lines mark local midnight. The observations and the AMIE-TIGCM calculations are plotted every universal time hour. Also plotted are the 12-day average of the observations and the time-averaged AMIE-TIGCM simulation in order to establish relative comparisons between the averaged behavior and that which occurred on March 28–29.

The only polar cap station in this set is Resolute Bay at 83°N magnetic latitude. Accurate modeling of high-latitude stations is very difficult because of the presence of such features as polar holes, tongues of ionization brought in by convection from the dayside that can later break into patches, high-latitude troughs, and auroral ionization [*Sojka et al.*, 1992; *Prölss*, 1995]. In addition, the polar cap is in a region of open field lines so plasma can continuously escape. The most striking thing about the observed peak electron density for Resolute Bay shown in Figure 4a is the fact that it is greater at night than during the day. The dashed line average between March 24 and April 4 reveals that while the daytime values are about average on March 28–29, the nighttime values for this period are much larger than usual. In fact, the nighttime values of March 28 and 29 are the largest of the entire month of March. The median behavior at Resolute Bay for the month of March 1992 (not shown) puts the peak electron density near 1500 LT, which would be more consistent with the model calculations. The model predicts the nighttime values fairly well in Figure 4a, but overestimates the daytime values by a factor of 2 to 3. Considering that these nighttime values are unusually large, it appears that

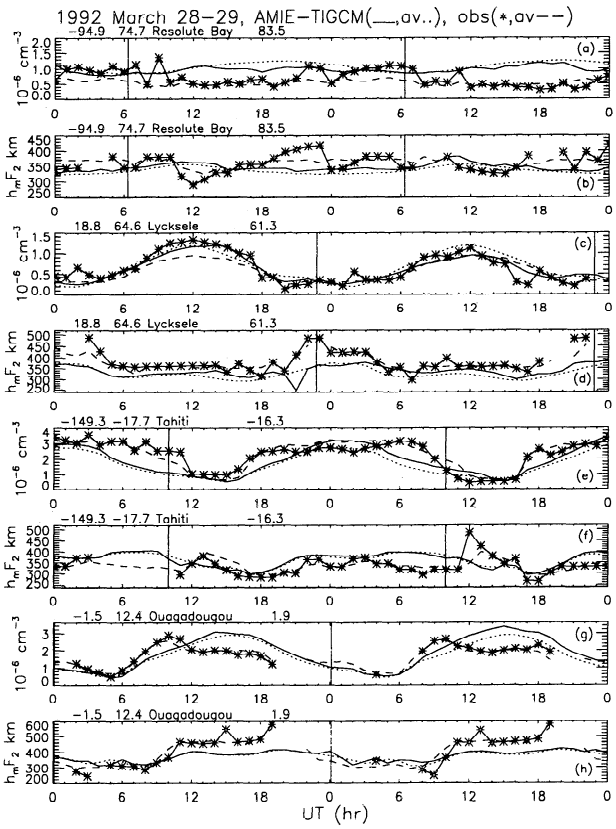

Figure 4. Ionosonde station observations for March 28-29, 1992, ordered in apex latitude, which is the number after the station name. The vertical lines show the location of local midnight and the asterisks are observations. The dashed line is the observational average between March 24 and April 4, 1992. The solid line is the calculations from the TIGCM using time-varying AMIE inputs while the dotted line uses time-averaged AMIE inputs. (a) $NmF2$ at Resolute Bay in 10^{-6} electrons/cm^3, (b) $hmF2$ at Resolute Bay in kilometers. (c) Same as Figure 4a except for Lycksele. (d) Same as Figure 4b except for Lycksele. (e) Same as Figure 4a except for Tahiti. (f) Same as Figure 4b except for Tahiti. (g) Same as Figure 4a except for Ouagadougou. (h) Same as Figure 4a except for Ouagadougou.

the simulation overestimates the peak electron density in this polar cap location by about a factor of 2 for all times. The most likely cause for this discrepancy is incorrect modeling of composition in the polar cap.

Comparisons were made of the neutral temperature and composition at 300 km from MSIS-90 [*Hedin*, 1991] and the time-averaged AMIE-TIGCM. The neutral temperatures were approximately equal except the MSIS temperatures were 25–50 K larger at high latitudes. The O density was about 75% of the MSIS O values except during the day at high latitudes when they were about equal. The major latitudinal differences were in the N_2 density, where the AMIE-TIGCM calculations were about 75% of the MSIS values at the equator, about 65% of the MSIS values during the day poleward of 25° geographic latitude, and 70% decreasing to 45% of the MSIS values during the night between 20° and

60°, respectively. If the MSIS model values are correct, then the resulting change in the O/N_2 ratio at 300 km for Resolute Bay at 74.7°N is a decrease of 65% during the day and a decrease of 60% at night resulting in similar decreases in the peak electron density. Such composition changes would be in the right direction to improve the comparison between the observations and calculations of the peak electron density at Resolute Bay. The *hmF*2 observations in Figure 4b are approximated by the model calculations, although there are deviations that could be due to incorrect specification of the polar cap electric field from AMIE.

Lycksele in Figures 4c and 4d is close to the auroral oval. The *NmF*2 is modeled well by the AMIE-TIGCM on both days and nights, although the calculated *hmF*2 is lower than the observations. The drop in *hmF*2 at 2100 UT on March 28 in the AMIE-TIGCM model is an indicator of auroral ionization at that time. The calculated daytime *NmF*2 is lower on March 29 than on March 28 and is lower than the time-averaged dotted line calculation. This decrease on March 29 is due to a smaller O/N_2 ratio.

Tahiti is in the equatorial anomaly and shows a maximum in the electron density in the premidnight region in Figure 4e. A premidnight maximum in *NmF*2 is observed for at least 1 day for all the stations that lie between 10° and 16° magnetic north or south. The premidnight peak in electron density is a consistent feature of the anomaly crest during solar maximum conditions, although the peak is just after noon in solar minimum. The present model runs do not reproduce this peak, possibly because the electric field model of *Richmond et al.* [1980] used in the simulations is an average model based mostly on solar minimum data.

Ouagadougou lies near the magnetic equator, and like the other stations within a few degrees of the equator, shows a peak electron density around 0900 LT in Figure 4g, followed by a noon bite-out and relatively flat values the rest of the afternoon. The noon bite-out of electron density is a common feature at these latitudes [e.g., *Prölss*, 1995]. All of the stations between ±10° magnetic latitude show much lower densities during the remainder of the day compared to the simulation. The observed *hmF*2 values are also much higher than those predicted by the model as shown in Figure 4h. At low latitudes, there is an anticorrelation of *hmF*2 and *NmF*2 [e.g., *Fesen et al.*, 1989; *Codrescu et al.*, 1992; *Prölss*, 1995]. The discrepancies between the model calculations and the observations could be the result of incorrect electric fields in the model.

Gravity Waves

Figure 5 is a plot of the observations on March 28-29 of *NmF*2, *hmF*2, and the servo-model ionosonde winds for Norfolk Island (29°S, 168°E) which is at a magnetic latitude of 35.7°S. The winds are positive toward the north or equatorward in the southern hemisphere. Figures 5b and 5c show clear evidence of gravity waves in the observations and calculations of *hmF*2 and the meridional wind at night, especially on March

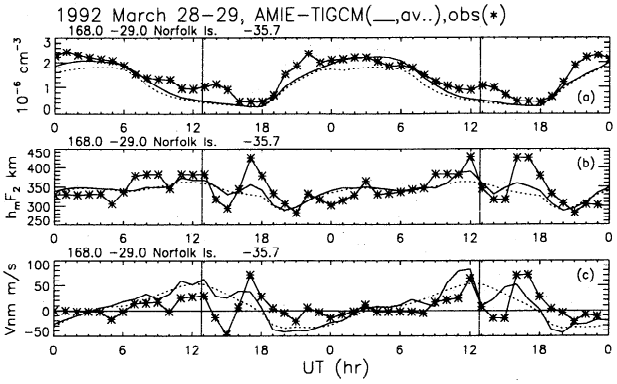

Figure 5. Same as Figure 4 except for Norfolk Island observations for March 28–29, 1992. The observational average was omitted for the sake of clarity. (a) *NmF*2 in 10^{-6} electrons/cm^3, (b) *hmF*2 in km, and (c) neutral wind positive toward magnetic north in meters per second.

29. This is consistent with the calculations of *Fuller-Rowell and Rees* [1981] and *Roble et al.* [1987], who showed that the largest transitory effects on the neutral wind were at night. The gravity waves are also evident at other southern hemisphere stations in this longitude sector from Hobart at 53.9°S magnetic latitude to Darwin at 22.2°S. The correspondence between the timing of the observed gravity waves and the calculated gravity waves is fairly close. By definition, the servo model gives no lag between the ionosonde winds and *hmF*2, but the AMIE-TIGCM results show lags of between 0 and 1 hours between initial peaks in the equatorward wind and increasing *hmF*2. This is consistent with estimates of the lag to be between 15 and 30 min [*Richards*, 1991]. Shifting the equatorward peaks in the ionosonde meridional wind earlier improves the comparison with the AMIE-TIGCM results. The gravity wave peaks and valleys in *hmF*2 are larger in the observations compared to the simulations. The magnitude of the gravity-wave-produced peaks in the inferred meridional wind are probably underestimated in these conditions of rapid change in *hmF*2 since servo models assume steady state conditions.

On both nights, there is an increase in the observed *NmF*2 following increases in *hmF*2, but there is no increase in the simulated *NmF*2 following increases in *hmF*2. This is in agreement with *Prölss* [1995], who states that increases in *hmF*2 at night are ineffective in raising the *NmF*2. However, a large time-varying downward O^+ flux in the TIGCM could increase the *NmF*2 at night, although time variations in the upper boundary O^+ flux are not at present in the model.

Figure 6 illustrates the waves in the neutral and ionized parameters as differences between the calculations from the AMIE-TIGCM run on March 29 compared to the time-averaged AMIE-TIGCM run. The plots cover the nighttime region for the longitude of 140°E around 380 km as a function of geographic latitude, where the magnetic equator is at approximately 10°N. Figure 6a shows the temperature differences which maximize in

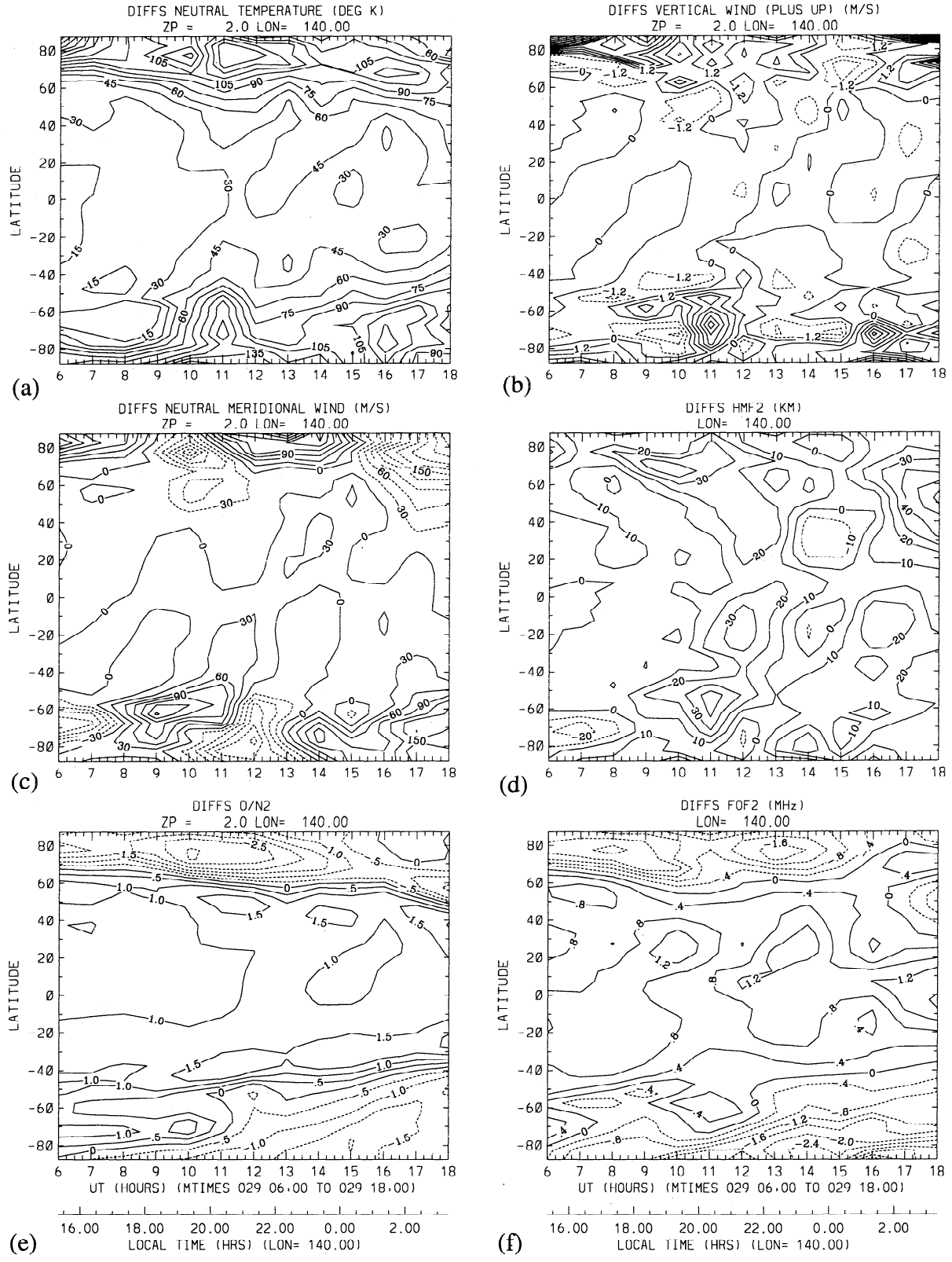

Figure 6. Plots of the differences at the +2 pressure surface near 380 km for the longitude of 140°E as a function of geographic latitude on March 29, 1992, between 0600 and 1800 UT. The differences are between the AMIE-TIGCM calculations for March 29 versus the time-averaged simulation. (a) Neutral temperature in kelvin, (b) neutral vertical wind in meters per second, (c) neutral meridional wind in meters per second, (d) height of the $F2$ peak electron density, $hmF2$, in kilometers, (e) O/N_2 ratio, and (f) critical frequency of the $F2$ peak electron density, $foF2$, in megahertz.

high latitudes. The Joule heating maxima at 1000 UT on March 29 in Figure 2c produce the neutral difference temperature maxima at 1100 UT in Figure 6a and the upwelling in Figure 6b. The strong upwelling in the southern hemisphere at 67.5°S brings N_2 from lower altitudes and is associated with the change from positive to negative differences in the O/N_2 ratio plotted in Figure 6e. The negative differences then drift toward lower latitudes at the rate of about 10° in 4 5 hours. The Joule heating maximizes in the dusk sector around 0900 UT near the longitude of 140°E in the southern hemisphere, triggering equatorward difference winds (positive) in Figure 6c at 57.5°S. The Joule heating in the northern hemisphere is split between the dusk sector and the dayside and triggers maximum equatorward difference winds (negative) in Figure 6c at 72.5°N at 1000 UT. These equatorward difference winds propagate to the equator, arriving between 1100 and 1200 UT for propagation times of between 1.5 and 2.5 hours. These propagation times from high latitudes to the equator are consistent with the calculation of 2 hours by *Roble et al.* [1987] and of 2.5 hours by *Richmond and Matsushita* [1975].

Figures 6b and 6c show that the converging difference winds at the equator between 1100 and 1200 UT are associated with downward difference vertical winds. These results are in agreement with similar difference plots for the TGCM analysis of the storm on March 22, 1979, described by *Roble et al.* [1987]. The converging winds at 1200 UT in Figure 6c are also associated with relative increases in the $hmF2$ on either side of the equator around 25° magnetic latitude (35°N, 15°S) shown in Figure 6d. Differences in $foF2$ are generally positive at low latitudes and negative at high latitudes, but the peaks in $hmF2$ near 25° magnetic latitude at 1200 UT are colocated with relative minima in $foF2$. There is then a relative increase in $foF2$ at the magnetic equator (10°N), while there is a relative decrease in $hmF2$. The anticorrelation of $NmF2$ and $hmF2$ in the lower latitudes is in agreement with observations and models [e.g. *Fesen et al.*, 1989; *Codrescu et al.*, 1992; *Prölss*, 1995]. However, the major variations of $foF2$ in midlatitude and high-latitude regions are strongly correlated with variations in the O/N_2 ratio plotted in Figure 6e which will be discussed in the next section.

Positive/Negative $NmF2$ Variations and O/N_2

The upper midlatitude stations shown in Figure 7 illustrate distinct longitudinal differences in the changes in the daytime $NmF2$ between March 28 and 29 and different deviations from their 12 or 2-day averages. We will look at the relative variations of $NmF2$ within this 12-day disturbed period and explain them in terms of O/N_2 variations. Of particular interest are the variations in the same longitude sector where the observed $NmF2$ values of Wallops Island in Figure 7b are only slightly larger on March 28 than its average, while in Figure 7c the $NmF2$ values at Ottawa further north are much larger than the average. In comparing the northern and southern hemisphere stations of Magadan and Hobart in Figures 7g and 7h, the observations for both days are different in each hemisphere with respect to their averages. In all cases where the AMIE-TIGCM time-averaged $NmF2$ values are different from the calculated $NmF2$ values on March 29, the higher values are the result of higher O/N_2 values on the constant pressure surface around 380 km. This is consistent with the difference results of Figures 6e and 6f, where changes in $foF2$ correlate well with variations in O/N_2. At 0600 UT on March 29 in Figure 6e, the difference in the O/N_2 ratio at Hobart (42.9°S, 147.3°E) is positive, which results in the larger $foF2$ in Figure 6f, and the larger $NmF2$ in Figure 7h compared to the time-averaged value. Magadan at (60.1°N, 151.0°E) is very close to the strong gradients in O/N_2 in Figure 6e, and shows only a slight increase in O/N_2 at 0600 UT on March 29 in Figure 7g relative to the time average.

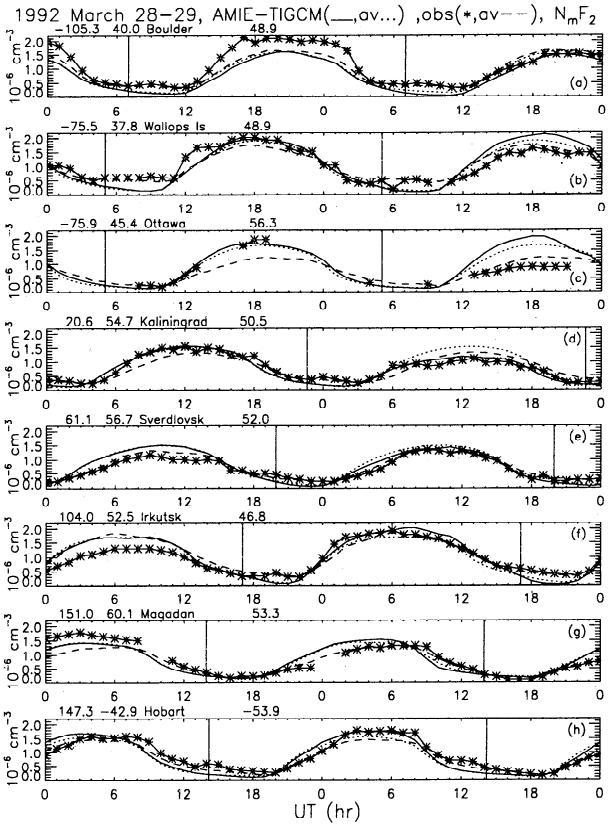

Figure 7. Same as Figure 4 except for $NmF2$ in 10^{-6} electrons/cm^3 for March 28–29, 1992, for stations between 46° and 56° apex latitude north or south. The stations are ordered in geographic longitude: (a) Boulder, (b) Wallops Island, (c) Ottawa, (d) Kaliningrad, (e) Sverdlovsk, (f) Irkutsk, (g) Magadan, and (h) Hobart.

Prölss [1993] states that most subauroral storm effects are negative with daytime ionization losses due to decreases in the O/N_2 ratio created in the night sector that move equatorward and last well into the next day before dissipating. Figure 8 is a plot of the percent difference in the O/N_2 ratio on March 29 compared to the time-averaged calculations as a function of universal time for the magnetic latitude of 52°N. The local times

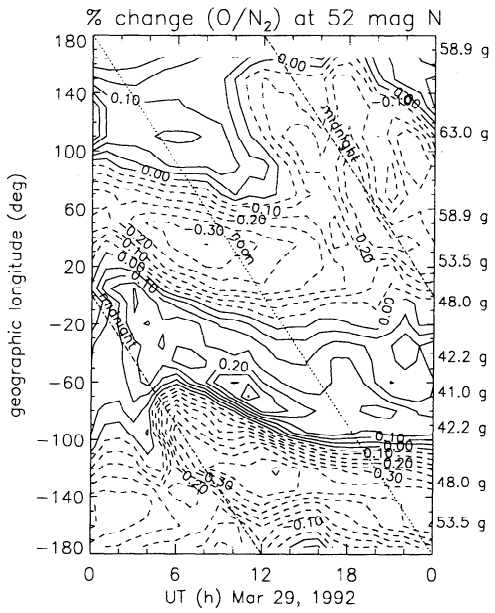

Figure 8. Percent change in the O/N_2 ratio on March 29 at the constant pressure level +2 near 380 km for the magnetic latitude of 52°N as a function of universal time and geographic longitude compared to the time-averaged simulation. The numbers on the right axis correspond to the geographic latitude.

of midnight and noon are shown as slanting dashed-dotted and dotted lines, respectively. The O/N_2 ratio on March 29 is decreased up to 45% and increased up to 35% compared to the time-averaged calculation. The minima are 75°–120° wide in longitude and tend to die away in the afternoon and early evening before being replaced with other minima. The minima in O/N_2 differences are about 2 hours earlier in universal time and at more eastward locations 5° further poleward. Heating events in the high-latitude dusk sector produce minima in O/N_2 which are moved equatorward by the meridional neutral winds and westward by the zonal neutral winds which follow the sunward ion convection. In addition, the minima parallel to the midnight line between 100° and 120°W is a reflection of successively westward longitudes rotating into a region of Joule heating in the dusk sector.

Figure 8 can be compared with the calculations of $NmF2$ in Figure 7. In particular, at the location of Ottawa at 76°W, the noon-time percent change in O/N_2 is positive, so the AMIE-TIGCM $NmF2$ at noon on March 29 in Figure 7c is larger than the time-averaged $NmF2$ although the observations show a negative response in $NmF2$ compared to the 12-day average. However, Ottawa is only 25° east of a region of large negative changes, which implies that the exact timing and location of the Joule heating was missed for this longitude. Apart from 76°W, the AMIE-TIGCM calculates the $NmF2$ in Figure 7 better on March 29 compared to March 28. This is probably due to the long residence times associated with O/N_2 decreases. Because the Joule heat impulses are not correctly modeled before March 28, the O/N_2 longitudinal asymmetries similar to those in Figure 8 will not be set up correctly. Excluding Ottawa, for the 12 stations between 47 and 57° magnetic latitude, the average $NmF2$ values for 5 hours around local noon are overestimated by AMIE-TIGCM by 15.3% on the first day and by 8.6% on the second day. This demonstrates the utility of using AMIE high-latitude inputs which in general improve the calculation of daytime $NmF2$ values on March 29 compared to March 28 in response to realistic local and universal time placement of Joule heating events.

Average Midlatitude Comparisons

The companion study by *Szuszczewicz et al.* [this issue] showed that the major disagreement between the climatological AMIE-TIGCM model run and the observations was the failure of the model to maintain the observed level of peak ionization at night. They attribute this failure to smaller model equatorward winds at night that lead to lower $hmF2$ heights, which in turn put the peak electron density in a region of higher loss rate. *Sica et al.* [1990] addressed the problem of the nighttime maintenance of the electron density in mid-latitudes for the solar minimum, quiet day of September 28, 1986, and concluded it could be maintained with strong equatorward winds, downward O^+ flux, or some combination of the two processes. In order to quantify the differences between the AMIE-TIGCM calculations and the observations for March 28–29 and to compare more easily with the companion paper of *Szuszczewicz et al.* [this issue], averages of $NmF2$, $hmF2$, and the meridional winds as a function of local time are plotted in Figure 9 for 33 stations (24 with $hmF2$) between 20° and 60° magnetic latitude.

From Figure 9a, the AMIE-TIGCM calculations of $NmF2$ are larger than the observations in the afternoon and smaller at night. Figure 9b plots the differences between the model and the observations as a percentage to show that the model overestimates $NmF2$ during the day by 5 to 15%, and underestimates $NmF2$ at 0300 LT by 45% or nearly a factor of 2. This is in general agreement with *Szuszczewicz et al.* [this issue].

Similarly, the model underestimates $hmF2$ by 35 km at midnight in Figure 9c (similar to Figure 5 for magnetic latitudes greater than 25° in *Szuszczewicz et al.* [this issue]) because the model $hmF2$ peaks 3–4 hours later than the observations. A shorter time discrepancy is seen in the nighttime equatorward winds shown in Figure 9d, where the model winds peak 1-2 hours later than the ionosonde winds. This is in contrast to data in the study by *Miller et al.* [1986] where the peak equatorward ionosonde winds usually followed peaks in the winds derived from the Millstone Hill and Arecibo incoherent scatter radars by 1–2 hours. In addition, there is a suggestion in the Fabry-Perot comparisons of the meridional winds in Figure 3e that the AMIE-TIGCM winds peak 1-2 hours later than the observations. The later AMIE-TIGCM equatorward winds produce the delayed peak in $hmF2$ between 0300 and 0400 LT in Figure 9c. The cause for the delay in the

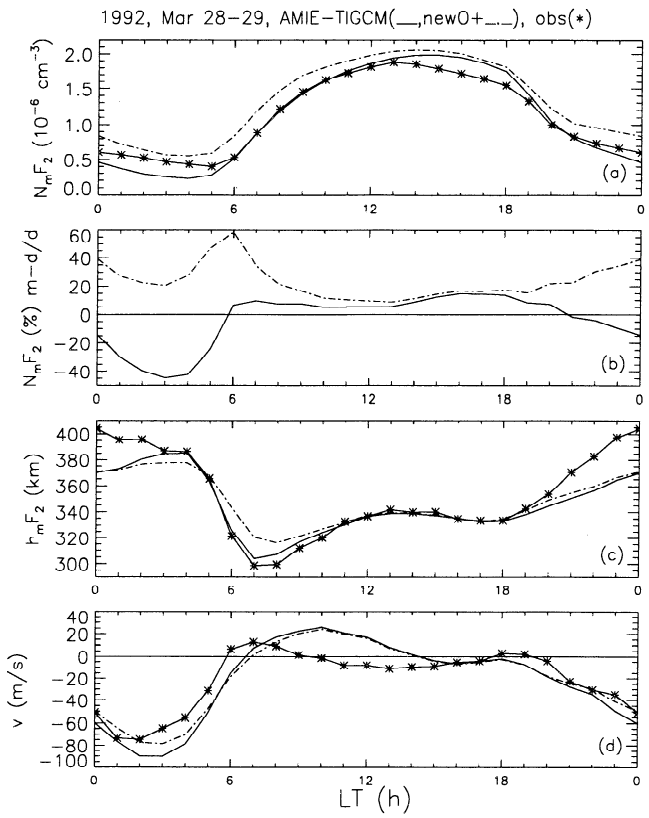

Figure 9. Average values on March 28–29, 1992, as a function of local time for ionosonde locations between 20° and 60° magnetic latitude. The solid lines are the regular AMIE-TIGCM simulation while the dashed-dotted lines include the revised O^+ flux specification of Figure 10. Asterisks are observations. (a) *NmF2* in 10^{-6} electrons/cm^3, (b) *NmF2* percent differences as (model-data)/data, (c) *hmF2* in kilometers, and (d) meridional neutral winds positive poleward in meters per second.

AMIE-TIGCM peak equatorward winds compared to observations is not known at this time.

Unlike the time-averaged calculations of the meridional wind shown in Figure 7 of *Szuszczewicz et al.* [this issue], the model winds for March 28–29 are always more equatorward than the ionosonde derived winds at night. The magnitude of the ionosonde winds is affected by the MSIS composition assumed. The winds were derived using constant values of the solar flux and *Ap* consistent with the entire SUNDIAL period. However, the solar fluxes for March 28–29 are larger, and have the effect on two stations around 50°N magnetic latitude of shifting the daytime velocities poleward by about 20 m/s to be in better agreement with the model results plotted in Figure 9d. Reducing the MSIS N_2 and O_2 densities at 300 km by factors of 2 and 3, respectively, to be in better agreement with the AMIE-TIGCM densities, had the effect on these two stations of shifting the winds equatorwards day and night between 15 and 35 m/s, with increases less than 20 m/s at the time of the equatorward peaks. Considering the uncertainties on the ionosonde derived winds due to changes in the solar flux and uncertainties in the density and the observed *hmF2*, the conclusion is that the magnitude of the model winds is comparable to the winds derived from ionosonde measurements. However, the timing of the peak equatorward wind is also a very significant factor.

To help determine the effects of timing and composition on *NmF2* and *hmF2*, several field line interhemispheric plasma (FLIP) model [*Richards and Torr*, 1988] runs were done at (55°N, 0°E) using the AMIE-TIGCM meridional winds averaged over the stations located between 47° and 57° magnetic latitude. When the input winds were shifted 2 hours earlier, the *NmF2* values were increased by a factor of 2 at 0400 LT, while *hmF2* increased 20 km around midnight compared to the control run using the same AMIE-TIGCM winds with no time shift. When the MSIS N_2 density was decreased by a factor of 2 at 300 km, the *NmF2* values doubled during the day and more than doubled by the end of the night, since the loss is exponential at night instead of linear. These runs show that an earlier peak in the nighttime equatorward winds can help bring AMIE-TIGCM *hmF2* and *NmF2* into agreement with observations at night. If, in addition, the AMIE-TIGCM composition at 300 km were brought into agreement with the MSIS-90 values described in the section about Resolute Bay, the effect on the O/N_2 ratio around 40° would be a 15% decrease during the day and a 60% decrease during the night which corresponds roughly to the same decrease in *NmF2*. The decrease during the day is approximately the right magnitude to bring the daytime AMIE-TIGCM *NmF2* into agreement with the observations in Figure 9b, but the extra decrease at night causes us to look at the effect of increasing the downward O^+ flux at night.

O^+ Fluxes at the Upper Boundary

Plasma flows to and from the plasmasphere are known to have a marked effect on *NmF2* and a small effect on *hmF2* [e.g., *Sica et al.*, 1990]. The effects are greatest at night when there is no competing solar ionization. During magnetic storms, the plasma in the outer plasmasphere is stripped away by convection electric fields leaving depleted or empty flux tubes [e.g., *Sica et al.*, 1990]. The difference between full and empty flux tubes can be a factor of two in *NmF2*, with full flux tubes producing more *NmF2* and larger downward O^+ fluxes. The O^+ flux is also a strong function of solar cycle.

The solid lines in Figure 10 plot the day and night O^+ fluxes used in the TIGCM at the upper boundary, which is approximately at 550 km for this period. Constant daytime and nighttime values are used, with linear interpolations made between these two constants during sunrise and sunset at zenith angles between 80° and 100°. The day/night fluxes are equal and opposite except for the region of the polar cap which is defined to be greater than 60° magnetic latitude for this purpose.

In Figure 8 of *Szuszczewicz et al.* [this issue], the O^+ flux at 550 km from the FLIP model for average conditions during the SUNDIAL period is plotted

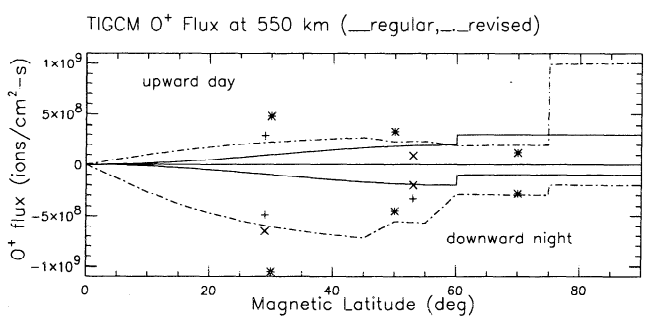

Figure 10. The day/night O^+ flux in units of ions/cm^2-s at the upper boundary of the TIGCM near 550 km. The asterisks are average 12-hour values of the flux from the FLIP model from Figure 8 of *Szuszczewicz et al.* [this issue]. These are fluxes at 550 km at 20°E for the conditions of March 1992 (Sa=180) using effective winds from the M3000 values of the International Reference Ionosphere. Millstone Hill measurements at 650 km evenly divided over 12 hours of upward and downward flux are marked as crosses for March 25–26, 1969 (Sa=180), and as a plus for March 21–22, 1969 (Sa=230). Arecibo measurements at 551 km approximated over 12 hours are marked as pluses for March 16–17, 1982 (Sa=228) and as a cross for April 20, 1982 (Sa=145). The dashed-dotted line is the revised TIGCM O^+ flux specification.

for 20°E longitude for magnetic latitudes close to 30°, 50°, and 70°. The fluxes are large and upward around sunrise and large and downward around sunset, with other local time variations that depend on longitude. The fluxes are downward longer than they are upward, with approximately equal average magnitudes. Since the day/night fluxes in the TIGCM persist for 12 hours during equinox conditions, the FLIP average fluxes were converted to 12-hour averages, where the magnitude of the downward flux was approximately twice that of the upward flux, and plotted as asterisks in Figure 10.

The FLIP average O^+ flux values are considerably larger than the standard TIGCM values, especially at the lower latitudes. Therefore incoherent scatter radar measurements were found for equinox, solar maximum conditions at Millstone Hill and Arecibo, which are located at 53°N and 29°N magnetic latitude, respectively. The O^+ flux is a product of the electron density and the vertical ion drift. *Evans* [1974] plotted values of the O^+ flux at 650 km for 1969. Two nights and one day were averaged and converted to 12-hour segments and plotted in Figure 10 as crosses for periods with lesser 10.7-cm solar flux, and as pluses for periods with larger 10.7-cm solar flux. Similarly, two nights and one day of Arecibo measurements in 1982 between 517 and 586 km were calculated, averaged, converted to 12-hour segments at 550 km and plotted in Figure 10. The observations are less than the FLIP values but larger than the TIGCM. Accordingly, we revised the O^+ fluxes in the TIGCM and these are shown as a dashed-dotted line in Figure 10. The polar cap is now defined to be above 75° magnetic latitude with large daytime upward fluxes along open field lines. The day/night ratio of the flux magnitude at lower latitudes is about 1/3.

Figure 9 shows the effect of the new O^+ fluxes as dashed-dotted lines. The model electron densities in Figures 9a and 9b are now greater than the observations at all times, with the greatest increases occurring at night. The effect on the meridional winds and $hmF2$ are much smaller. The increased electron density increases the ion drag and so decreases the meridional winds by up to 15 m/s at night in Figure 9d. The reduced winds in turn lead to $hmF2$ values in Figure 9c which are about 8 km lower around 0400 LT and about 16 km higher around 0700 LT. At Resolute Bay at 83.5°N magnetic latitude, the daytime upward flux was increased over a factor of 3, but the effect was only a 12% decrease in $NmF2$ at best because of the dominance of the solar production of ionization. At low latitudes, the $NmF2$ was increased by about 10% at all times. A more realistic local time dependence of the O^+ flux would probably have smaller effects after midnight when the downward flux is relatively small compared to the initial sunset peak.

Summary and Conclusions

This study has described how the AMIE technique is used to derive auroral patterns, which are essential inputs to the TIGCM. Using AMIE high-latitude inputs in the TIGCM improves the universal and local time placement of Joule heating events and ion drag momentum sources which launch gravity waves and change the O/N_2 ratio within a local longitude sector. The total hemispheric Joule heating from the TIGCM is 5–20 GW larger in the hemisphere where the magnetic pole is tilted toward the sun, where the largest differences are associated with the largest electric fields.

The AMIE-TIGCM calculations help to interpret the Fabry-Perot observations at Watson Lake within auroral arcs which move the emission peak to lower altitudes. Making comparisons at the proper altitude improves the correspondence with the horizontal neutral winds. There is a suggestion that the observed equatorward winds peak 1-2 hours earlier than the model calculations. The AMIE-TIGCM vertical winds are unable to reproduce the rapid variations and large magnitudes in the observations because of the large grid spacing used.

Many gravity waves appeared in the AMIE-TIGCM results, with some specific waves found in nighttime observations of the $hmF2$ and ionosonde meridional winds. The postmidnight increases in $NmF2$ observed at Norfolk Island and other locations were not replicated by calculations of the AMIE-TIGCM, although a strong downward O^+ flux at night over approximately an hour or so could raise the $NmF2$. At low latitudes, gravity waves in the calculated $NmF2$ were anticorrelated with peaks in the $hmF2$ around ±25° magnetic latitude produced by equatorward difference winds that propagated from high latitudes to the equator in about 2 hours. Above about 40° latitude, the major influence on variations in $NmF2$ were long-lasting longitudinal asymmetries in the O/N_2 ratio. Joule heating events produce

minima in the O/N_2 ratio that move 5° equatorward in about 2 hours. There is westward movement of the minima due to westward winds in the premidnight sector at high latitudes, and the rotation of more westward locations into a region of on-going Joule heating. Gravity wave and O/N_2 changes were different in the two hemispheres at similar longitudes because of differences in the Joule heating.

The AMIE-TIGCM calculations of *NmF2* were compared with observations at various magnetic latitudes. The single polar station of Resolute Bay showed much larger model *NmF2* values during the day, and also at night on the average. The model *NmF2* could be substantially reduced if the AMIE-TIGCM N_2 density were doubled to be more like MSIS. Comparisons at midlatitudes showed underestimates of *NmF2* by a factor of 2 at 0300 LT. These underestimates were converted to overestimates of about 30% at midlatitudes between 2200 and 0700 LT by increasing the downward nighttime O^+ flux by factors of 2 to 6, values that are consistent with averaged incoherent scatter radar observations during solar maximum. However, a realistic local time variation in the O^+ flux with a large upward flux around sunrise would reduce the excess *NmF2* around 0600 local time while a large downward flux around sunset and low fluxes thereafter might be sufficient to maintain the observed levels of ionization. Agreement was not complete at the low-latitude stations where electric fields are expected to be important and where the empirical model of *Richmond et al.* [1980] that was used may be inadequate for the conditions simulated.

Comparisons of the ionosonde-derived winds between 20° and 60° magnetic latitude showed that the AMIE-TIGCM winds were more poleward during the day and more equatorward at night. The differences could be reduced if the AMIE-TIGCM winds were shifted 1–2 hours earlier, especially after midnight. Such a shift in the timing of the winds would also improve the 35 km discrepancy in the *hmF2* at midnight and raise the *NmF2* by up to a factor of 2 after midnight. Global comparisons at 300 km showed that if the AMIE-TIGCM composition were more like MSIS, the O/N_2 ratio in midlatitudes would be about 15% less during the day and about 60% less at night, leading to reduced *NmF2* values. A combination of composition and local time dependent O^+ flux changes should be investigated further as well as mechanisms to move the equatorward peak winds earlier. Most of the discrepancies between the model and observations may be rectified by a better physical description of magnetosphere/ionosphere interactions within the TIGCM.

This study has pointed out successes and failures in the model that require improvement in the modeling of aeronomic processes. Further campaign studies of this type should help improve the model performance for the ultimate goal of space weather studies. The present correspondence between data and model calculations for March 28–29, 1992, is remarkably good, but future studies can be carried out using the more advanced electrodynamics TIE-GCM model described by *Richmond et al.* [1992] which is being validated against climatological models and observations.

Acknowledgments. The Arecibo incoherent scatter radar measurements and the Watson Lake Fabry-Perot measurements were taken from the CEDAR (Coupling, Energetics and Dynamics of Atmospheric Regions) Data Base at the National Center for Atmospheric Research (NCAR) which is supported by the National Science Foundation (NSF). The Arecibo Observatory is operated by Cornell University under cooperative agreement with NSF. The Watson Lake Fabry Perot is operated by the University of Michigan with support from NSF and the US Air Force. We also thank all the institutions and agencies in each of the countries that participated in this investigation. This study was supported in part by the Space Physics Division of the National Aeronautics and Space Administration (NASA) under contract NASW-4755 with the Science Applications International Corporation (SAIC). P. Richards would like to acknowledge NSF grant ATM-9523786.

The Editor thanks M. H. Rees and C. G. Fesen for their assistance in evaluating this paper.

References

Ahn, B.-H., R. M. Robinson, Y. Kamide, and S.-I. Akasofu, Electric conductivities, electric fields and auroral energy injection rate in the auroral ionosphere and their empirical relations to the horizontal magnetic disturbances, *Planet. Space Sci., 31*, 641-653, 1983.

Blanc, M., and A. D. Richmond, The ionospheric disturbance dynamo, *J. Geophys. Res., 85*, 1669-1686, 1980.

Burns, A. G., T. L. Killeen, G. R. Carignan, and R. G. Roble, Large enhancements in the O/N_2 ratio in the evening sector of the winter hemisphere during geomagnetic storms, *J. Geophys. Res., 100*, 14,661-14,671, 1995a.

Burns, A. G., T. L. Killeen, W. Deng, G. R. Carignan, and R. G. Roble, Geomagnetic storm effects in the low- to middle-latitude upper thermosphere, *J. Geophys. Res., 100*, 14,673-14,691, 1995b.

Chenette, D. L., D. W. Datlowe, R. M. Robinson, T. L. Schumaker, R. R. Vondrak, and J. D. Winningham, Atmospheric energy input and ionization by energetic electrons during the geomagnetic storm of 8-9 November 1991, *Geophys. Res. Lett., 20*, 1323-1326,1993.

Codrescu, M. V., R. G. Roble, and J. M. Forbes, Interactive ionosphere modeling: A comparison between TIGCM and ionosonde data, *J. Geophys. Res., 97*, 8591-8600, 1992.

Crowley, G., B. A. Emery, R. G. Roble, H. C. Carlson, and D. J. Knipp, Thermospheric dynamics during September 18-19, 1984, 1, Model simulations, *J. Geophys. Res., 94*, 16,925-16,944, 1989a.

Crowley, G., B. A. Emery, R. G. Roble, H. C. Carlson, J. E. Salah, V. B. Wickwar, K. L. Miller, W. L. Oliver, R. G. Burnside, and F. A. Marcos, Thermospheric dynamics during September 18-19, 1984, 2, Validation of the NCAR thermospheric general circulation model, *J. Geophys. Res., 94*, 16,945-16,959, 1989b.

Dickinson, R. E., E. C. Ridley, and R. G. Roble, A three-dimensional, time-dependent general circulation model of the thermosphere, *J. Geophys. Res., 86*, 1499-1512, 1981.

Dickinson, R. E., E. C. Ridley, and R. G. Roble, Thermospheric general circulation with coupled dynamics and composition, *J. Atmos. Sci., 41*, 205-219, 1984.

Dudeney, J. R., The accuracy of simple methods for determining the height of the maximum electron concentration of the *F*2-layer from scaled ionospheric characteristics, *J. Atmos. Terr. Phys., 45*, 629-640, 1983.

Evans, J. V., *Millstone Hill Thomson Scatter Results for 1969, Techn. Rep. 513*, 139 pp., Lincoln Lab. Mass. Inst. of Technol., Cambridge, July 1974.

Fesen, C. G., R. E. Dickinson, and R. G. Roble, Simulation of the thermospheric tides at equinox with the National Center for Atmospheric Research thermospheric general circulation model, *J. Geophys. Res., 91*, 4471-4489, 1986.

Fesen, C. G., G. Crowley, and R. G. Roble, Ionospheric efects at low latitudes during the March 22, 1979, geomagnetic storm, *J. Geophys. Res., 94*, 5405-5417, 1989.

Forbes, J. M., R. G. Roble, and F. A. Marcos, Thermospheric dynamics during the March 22, 1979, magnetic storm, 2, Comparisons of model predictions with observations, *J. Geophys. Res., 92*, 6069-6081, 1987.

Fuller-Rowell, T. J., and D. S. Evans, Height-integrated Pedersen and Hall conductivity patterns inferred from the TIROS-NOAA satellite data, *J. Geophys. Res., 92*, 7606-7618, 1987.

Fuller-Rowell, T. J., and D. Rees, A three-dimensional, time-dependent simulation of the global dynamical response of the thermosphere to a geomagnetic substorm, *J. Atmos. Terr. Phys., 43*, 701-721, 1981.

Hedin, A. E., Extension of the MSIS thermosphere model into the middle and lower atmosphere, *J. Geophys. Res., 96*, 1159-1172, 1991.

Heelis, R. A., J. K. Lowell, and R. W. Spiro, A model of the high-latitude ionospheric convection pattern, *J. Geophys. Res., 87*, 6339-6345, 1982.

Hernandez, G., and R. G. Roble, Direct measurements of nighttime thermospheric winds and temperatures, 2, Geomagnetic storms, *J. Geophys. Res., 81*, 5173-5181, 1976.

Hernandez, G., and R. G. Roble, Thermospheric nighttime neutral temperature and winds over Fritz Peak Observatory: Observed and calculated solar cycle variation, *J. Geophys. Res., 100*, 14,647-14,659, 1995.

Knipp, D. J., et al., Ionospheric convection response to slow, strong variations in a northward Interplanetary Magnetic Field: A case study for January 14, 1988, *J. Geophys. Res., 98*, 19,273-19,292, 1993.

Lu, G., A. D. Richmond, B. A. Emery, and R. G. Roble, Magnetosphere-ionosphere-thermosphere coupling: Effect of neutral winds on energy transfer and field-aligned current, *J. Geophys. Res., 100*, 19,643-19,659, 1995.

Lu, G., B. A. Emery, A. Rodger, M. Lester, J. Taylor, D. S. Evans, M. Ruohoniemi, W. F. Denig, O. de la Beaujardiere, R. A. Frahm, J. D. Winningham, and D. L. Chenette, High-latitude ionospheric electrodynamics as determined by the assimilative mapping of ionospheric electrodynamics procedure for the conjunctive SUNDIAL/ATLAS 1/GEM period of March 28-29, 1992, *J. Geophys. Res.*, this issue.

Miller, K. L., D. G. Torr, and P. G. Richards, Meridional winds in the thermosphere derived from measurement of $F2$ layer height, *J. Geophys. Res., 91*, 4531-4535, 1986.

Miller, K. L., P. G. Richards, and H. Y. Wu, A global-scale study of meridional winds and electron densities in the F region during the SUNDIAL 1987 campaign, *Ann. Geophys., 11*, 572-584, 1993.

Mizera, P. F., and D. S. Evans, Simultaneous measurements of polar cap electron distributions in opposite hemispheres, *J. Geophys. Res., 91*, 9007-9011, 1986.

Price, G. D., R. W. Smith, and G. Hernandez, Simultaneous measurements of large vertical winds in the upper and lower thermosphere, *J. Atmos. Terr. Phys., 57*, 631-643, 1995.

Prölss, G. W., On explaining the local time variation of ionospheric storm effects, *Ann. Geophys., 11*, 1-9, 1993.

Prölss, G. W., Ionospheric F region storms, in *Handbook of Atmospheric Electrodynamics*, vol II, edited by H. Volland, pp. 195-248, CRC Press, Boca Raton, Fla., 1995.

Rees, M. H., and R. G. Roble, Excitation of $O(^1D)$ atoms in aurorae and emission of the [OI] 6300-A line, *Can. J. Phys., 64*, 1608-1613, 1986.

Reiff, P. H., and J. G. Luhmann, Solar wind control of the polar-cap voltage, in *Solar Wind-Magnetosphere Coupling*, edited by Y. Kamide and J. A. Slavin, pp. 453-476, Terra Sci., Tokyo, 1986.

Reiff, P. H., R. W. Spiro, and T. W. Hill, Dependence of polar cap potential drop on interplanetary parameters, *J. Geophys. Res., 86*, 7639-7648, 1981.

Rich, F. J., M. S. Gussenhoven, and M. E. Greenspan, Using simultaneous, particle and field observations on a low altitude satellite to estimate Joule heat energy flow into the high-latitude ionosphere, *Ann. Geophys., 5*, 527-534, 1987.

Richards, P. G., An improved algorithm for determining neutral winds from the height of the $F2$ peak electron density, *J. Geophys. Res., 96*, 17,839-17,846, 1991.

Richards, P. G., and D. G. Torr, Ratios of photoelectron to EUV ionization rates for aeronomic studies, *J. Geophys. Res., 93*, 4060-4066, 1988.

Richmond, A. D., and Y. Kamide, Mapping electrodynamic features of the high-latitude ionosphere from localized observations: Technique, *J. Geophys. Res., 93*, 5741-5759, 1988.

Richmond, A. D., and S. Matsushita, Thermospheric response to a magnetic substorm, *J. Geophys. Res., 80*, 2839-2850, 1975.

Richmond, A. D., et al., An empirical model of quiet day ionospheric electric fields at middle and low latitudes, *J. Geophys. Res., 85*, 4658-4664, 1980.

Richmond, A. D., et al., Mapping electrodynamic features of the high-latitude ionosphere from localized observations: Combined incoherent scatter radar and magnetometer measurements for January 18-19, 1984, *J. Geophys. Res., 93*, 5760-5776, 1988.

Richmond, A. D., E. C. Ridley, and R. G. Roble, A thermosphere/ionosphere general circulation model with coupled electrodynamics, *Geophys. Res. Lett. 19*, 601-604, 1992.

Robinson, R. M., R. R. Vondrak, K. Miller, T. Dabbs, and D. Hardy, On calculating ionospheric conductances from the flux and energy of precipitating electrons, *J. Geophys. Res., 92*, 2565-2569, 1987.

Roble, R. G., Energetics of the mesosphere and thermosphere, in *The Upper Mesosphere and Lower Thermosphere: A Review of Experiment and Theory, Geophys. Monogr. Ser.*, vol. 87, edited by R. M. Johnson and T. L. Killeen, pp. 1-21, AGU, Washington, D. C., 1995.

Roble, R. G., and E. C. Ridley, An auroral model for the NCAR thermospheric general circulation model (TGCM), *Ann. Geophys., 5*, 369-382, 1987.

Roble, R. G., A. D. Richmond, W. L. Oliver and R. M. Harper, Ionospheric effects of the gravity wave launched by the September 18, 1974, sudden commencement, *J. Geophys. Res., 83*, 999-1009, 1978.

Roble, R. G., J. M. Forbes, and F. A. Marcos, Thermospheric dynamics during the March 22, 1979, magnetic storm, 1, Model simulations, *J. Geophys. Res., 92*, 6045-6068, 1987.

Roble, R. G., E. C. Ridley, A. D. Richmond, and R. E. Dickinson, A coupled thermosphere/ionosphere general circulation model, *Geophys. Res. Lett., 15*, 1325-1328, 1988.

Sica, R. J., R. W. Schunk, and P. J. Wilkinson, A study of the undisturbed mid-latitude ionosphere using simultaneous multiple site ionosonde measurements during the Sundial-86 campaign, *J. Geophys. Res., 95*, 8271-8279, 1990.

Sipler, D. P. M. A. Biondi, and M. E. Zipf, Vertical winds in the midlatitude thermosphere from Fabry-Perot Interferometer measurements, *J. Atmos. Terr. Phys., 57*, 621-629, 1995.

Smith, R. W., and G. Hernandez, Vertical winds in the thermosphere within the polar cap, *J. Atmos. Terr. Phys., 57*, 611-620, 1995.

Sojka, J. J., R. W. Schunk, D. Rees, T. J. Fuller-Rowell, R. J. Moffett, and S. Quegan, Comparison of the USU ionospheric model with the UCL-Sheffield coupled thermospheric-ionospheric model, *Adv. Space Res., 12*, (6), 89-92, 1992.

Szuszczewicz, et al., *F* region climatology during the SUNDIAL/ATLAS 1 campaign of March 1992: Model-measurement comparisons and cause-effect relationships, *J. Geophys. Res.*, this issue.

VanZandt, T. E., W. L. Clark, and J. M. Warnock, Magnetic apex coordinates: A magnetic coordinate system for the ionospheric *F*2 layer, *J. Geophys. Res., 77*, 2406-2411, 1972.

Wilkinson, P. J., Scaling errors in ionospheric characteristics, *Ionosonde Network Advisory Group Bulletin*, vol. 27, p. 20, World Data Cent. A for Solar Terr. Phys., U. S. Dep. of Comm., Natl. Oceanic and Atmos. Admin., Boulder, Colo., 1978.

Wilkinson, P. J., R. Schunk, R. Hanbaba, and H. Mori, Interhemispheric comparison of SUNDIAL *F* region data with global scale ionospheric models, *Ann. Geophys., 6*, 31-38, 1988.

Wilkinson, P. J., E. P. Szuszczewicz, and R. G. Roble, Measurements and modelling of intermediate, descending, and sporadic layers in the lower ionosphere: Results and implications for global-scale ionospheric-thermospheric studies, *Geophys. Res. Lett., 19*, 95-98, 1992.

Wilkinson, P. J., P. Richards, K. Igarashi, and E. P. Szuszczewicz, Ionospheric climatology and weather in the Australian-Japanese sector during the SUNDIAL/ATLAS 1 campaign, *J. Geophys. Res.*, this issue.

M. Abdu, Divisao de Aeronmia, Instituto Nacional de Pesquisas Espaciais, CP 515, Sao Jose dos Campos SP 12200, Brazil (e-mail: inpedae@fpsp.fapesp.br attn: M. Abdu).

D. L. Chenette, Lockheed Palo Alto Research Laboratory, Department 91 20 Bldg. 255, 3251 Hanover St., Palo Alto, CA 94304-1191 (e-mail: chenette@pemaxs.space.lockheed.com).

W. F. Denig and F. J. Rich, Geophysics Directorate, Phillips Laboratory, Hanscom Air Force Base, MA 01731 (e-mail: denig@plh.af.mil; rich@plh.af.mil).

B. A. Emery, G. Lu, A. D. Richmond, and R. G. Roble, High Altitude Observatory, National Center for Atmospheric Research, P. O. Box 3000, Boulder, CO 80307-3000 (e-mail: emery@ncar.ucar.edu; ganglu@ncar.ucar.edu; richmond@ncar.ucar.edu; roble@ncar.ucar.edu).

D. S. Evans, Space Environment Center, National Oceanic and Atmospheric Administration, 325 Broadway, Boulder, CO 80303 (e-mail: devans@sel.noaa.gov).

R. Hanbaba, CNET, Lab PT1 Spi, Route de Tregastal B P 40, Lannion, Cedex F-22301, France (e-mail: hanbaba@lannion.cnet.fr).

K. Igarashi, Upper Atmosphere Section, Communications Research Laboratory, Ministry of Posts and Telecommunications, 4-2-1 Nukui Kitamachi Koganei-shi, Tokyo 184, Japan (e-mail: igarashi@crl.geo.jp).

P. Jiao, China Research Institute of Radiowave Propagation, P. O. Box 138197, Xinxiang, Henan, 453003, China (e-mail: crirp@mimi.cnc.ac.cn attn: P. Jiao).

K. L. Miller, CASS, Utah State University, Logan, UT 84322-4405 (e-mail: miller@logan.cass.usu.edu).

R. Niciejewski, Space Physics Research Laboratory, University of Michigan, 2455 Hayward, Ann Arbor, MI 48109-2143 (e-mail: niciejewski@sprlc.sprl.umich.edu).

K. F. O'Loughlin, National Geophysical Data Center, National Oceanic and Atmospheric Administration, 325 Broadway, Boulder, CO 80303 (e-mail: kfo@ngdc.noaa.gov).

S. Pulinets, Institute of Terrestrial Magnetism, Ionosphere and Radiowave Propagation, IZMIRAN, Moscow Region, 142092 Troitsk, Russia (e-mail: pulse@charley.izmiran.rssi.ru).

B. M. Reddy, Radio Science Division, National Physical Laboratory, Dr. K. S. Krishnan Rd., New Delhi 110012, India.

P. G. Richards, Computer Science Department, University of Alabama, Huntsville, AL 35899 (e-mail: richardsp@cspar.uah.edu).

E. P. Szuszczewicz, Laboratory for Atmospheric and Space Science, Science Applications International Corporation, 1710 Goodridge Drive, McLean, VA 22102 (e-mail: szusz@mclapo.saic.com).

P. Wilkinson, IPS Radio and Space Services, P. O. Box 5606, West Chatwood NSW 2057, Australia (e-mail: phil@ipso.ips.oz.au).

(Received February 26, 1996; revised April 22, 1996;
accepted April 23, 1996.)